

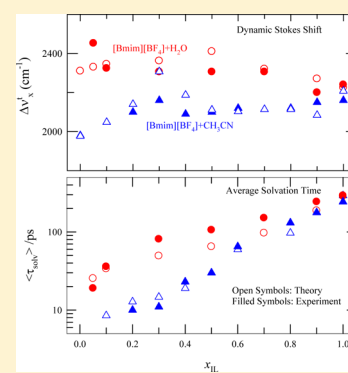
Composition Dependent Stokes Shift Dynamics in Binary Mixtures of 1-Butyl-3-methylimidazolium Tetrafluoroborate with Water and Acetonitrile: Quantitative Comparison between Theory and Complete Measurements

Snehasis Daschakraborty and Ranjit Biswas*

Department of Chemical, Biological and Macromolecular Sciences, S. N. Bose National Centre for Basic Sciences, JD Block, Sector III, Salt Lake, Kolkata 700098, India

S Supporting Information

ABSTRACT: Here we predict, using a semimolecular theory, the Stokes shift dynamics of a dipolar solute in binary mixtures of an ionic liquid (IL), 1-butyl-3-methylimidazolium tetrafluoroborate ([Bmim][BF₄]), with water (H₂O) and acetonitrile (CH₃CN), and compare with the experimental results. The latter are from the recent measurements that combined broad-band fluorescence up-conversion (FLUPS) with time-correlated single photon counting (TCSPC) techniques and used coumarin 153 (C153) as a solute probe. Nine different compositions of ([Bmim][BF₄] + H₂O) and ([Bmim][BF₄] + CH₃CN) binary mixtures are considered for the extensive comparison between theory and experiments. Two separate model calculations have been performed using the available experimental frequency dependent dielectric function, $\epsilon(\omega)$. These calculations semi-quantitatively reproduce the experimentally observed (i) IL mole fraction dependence of dynamic Stokes shifts in these mixtures, (ii) composition dependence of average fast, slow, and solvation times, (iii) viscosity dependence of slow times, and (iv) the nonlinear dependence of average solvation times on experimental inverse conductivity. Variations of the calculated dynamics on water dipole moment values (gas phase or liquid phase) and sensitivity to different measurements of $\epsilon(\omega)$ for ([Bmim][BF₄] + H₂O) mixtures are examined. In addition, the importance of the missing contribution to experimental $\epsilon(\omega)$ from high frequency collective solvent intermolecular modes for generating the experimentally observed sub-picosecond solvation response in these (IL + polar solvent) binary mixtures has been explored.



I. INTRODUCTION

Binary mixtures of ILs with water and other common polar solvents offer a unique opportunity for exploring how a chemical event responds as the medium transforms from dilute electrolyte solutions in polar solvents to the molten electrolyte itself by simply altering the mixture composition. If a simple chemical reaction is used as a probe, the rate of such a reaction registers the consequent effects due to a change in mixture composition because the reaction rate couples to the organizational dynamics of the surrounding medium.^{1–3} Addition of cosolvent strongly affects the transport properties of an IL, and thus, a reaction rate gets affected via the modification of the medium reorganization time scales. Moreover, addition of co-solvent will affect the static dielectric constant (ϵ_0) of IL, providing another avenue for influencing a reaction via the modification of the reaction barrier. These two factors are critical for engineering a designer reaction medium for tailoring a particular reaction that can yield a specific reaction product. Such a technological importance stimulates the efforts for studying (IL + common polar solvent) binary mixtures in detail. Apart from this application potential, basic scientific interest stems from the inquisition that how and to what extent the reorganization dynamics of systems containing

ILs is linked to the frequency dependent dielectric response, $\epsilon(\omega)$. Note a relation between solvation response and $\epsilon(\omega)$ is well understood for common dipolar solvents.^{4–13} A similar connection for pure ILs is currently under intense investigation and scrutiny.^{14–32} In such a scenario, a systematic theoretical study connecting solvation response and experimental $\epsilon(\omega)$ of (IL + polar solvent) binary mixtures may provide not only critical information on how medium dynamics and $\epsilon(\omega)$ are coupled in such binary mixtures but can also generate understanding on the origin of ultrafast response in neat ILs which is a subject of much debate now.^{14–23,25–38} The present study aims at exploring several aspects pertaining to dynamics of (IL + polar solvent) binary mixtures which may provide some clue for disentangling this complex issue.

Stokes shift dynamics in (IL + dipolar solvent) binary mixtures was studied earlier using temporal resolutions much broader than that required for complete detection of full dynamics of these systems.^{39–43} Consequently, a significant portion of the initial fast dynamics was reported missing and, in

Received: September 19, 2013

Revised: January 17, 2014

Published: January 22, 2014

some cases, entire mixture composition was not experimentally explored. Hence, the information available from these measurements remained largely incomplete, inviting further studies with sharper resolution. Nevertheless, these studies provided estimates of dynamic shift for a dissolved dipolar solute probe in (IL + dipolar solvent) mixtures and, more importantly, generated a sense of reorganization time scales inherent to them.^{39–43} An early simulation study of an aqueous mixture of an imidazolium IL revealed the importance of environmental exchange for energy relaxation to be complete.⁴⁴ We have already developed a semimolecular theory for understanding the dynamic Stokes shift measurements of (IL + dipolar solvent) binary mixtures where dynamic shift has been modeled as a sum total of three mutually independent interaction contributions, namely, solute–IL dipolar interaction, solute–IL dipole–ion interaction, and solute–solvent (added) dipolar interaction.¹⁸ However, nonavailability of complete measurements has prevented a rigorous test of this semimolecular theory and the subsequent refinement. Recently, Zhang et al.²³ have combined (FLUPS + TCSPC) techniques to measure complete Stokes shift dynamics using C153 for ([Bmim][BF₄] + H₂O) binary mixtures. Subsequently, Liang et al.⁴⁵ have employed the same combined technique to measure the dynamic solvation response in ([Bmim][BF₄] + CH₃CN) systems. In addition, experimental $\epsilon(\omega)$ over a broad frequency range ($0.2 \leq \nu/\text{GHz} \leq 89$) are now available for these mixtures.^{23,46} Naturally, these high quality, composition dependent experimental data for both solvation dynamics and $\epsilon(\omega)$ stimulate further study, enabling a comprehensive test of our semimolecular theory for its predictive ability. A quantitative comparison between theory and experiments at this juncture will serve as important feedback for further refinement, if necessary, over the model already employed.

Here we have performed two model calculations for binary mixtures of [Bmim][BF₄] with H₂O and CH₃CN. The first model views the mixtures as fully dissociated ions being dispersed in an “effective” dipolar medium constituted by the dipolar ions of the IL and the added dipolar solvent molecules. In such an approximate description, dipolar interactions between the dipolar solute and the dipolar ions of the IL and that between the solute and the added dipolar solvent molecules are replaced by a single effective dipolar interaction where the dipole moment of the effective dipolar particle is determined by the mole fraction dependent experimental^{23,46} ϵ_0 and size by the mole fraction weighted van der Waals volumes of the dipolar ion and the added dipolar solvent molecule. The total solute–IL interaction in such an effective medium (EM) is therefore composed of two components: dipole–dipole interaction between the dipolar solute and the effective dipolar particles and dipole–ion interaction between the dipolar solute and the dispersed ions. Note the determination of effective dipole moment and particle size by the above manner is motivated by the experimentally observed near-linear dependence of spectral frequencies on volume fraction.²³ In EM calculations, experimental $\epsilon(\omega)$ ^{23,46} have been used directly as inputs. The solution heterogeneity aspect^{47–54} is therefore partially incorporated in EM predicted dynamics. In addition, use of experimental $\epsilon(\omega)$ of mixtures partially incorporates the interaction between IL and the added solvent molecules in the EM calculations.

The other model, which recognizes the separate identity of the interaction between the solute and the added solvent molecules, describes the total solute–medium interactions as a

sum of three independent contributions: the solute–dipolar ion dipole–dipole interaction, solute–ion dipole–ion interaction, and solute–solvent dipole–dipole interaction. This we term as a “separate medium” (SM) which allows, within certain approximations, determination of a piece-wise contribution to the total shift and dynamics. Here also a given IL is considered to be fully dissociated, and the interaction between IL and added dipolar solvent molecules enters in this model via the use of experimental viscosity.^{23,45} The number densities also change according to mixture composition. This formalism then makes use of experimental $\epsilon(\omega)$ of neat components for the relevant calculations and, therefore, does not include, even indirectly, the solution structural aspect of real (IL + dipolar solvent) binary mixtures. This and nonincorporation of inhomogeneous density distribution around a dissolved solute (that is, spatial heterogeneity^{47–54}) may have some impact on the final calculated results and the subsequent comparisons with experiments.

II. THEORY AND CALCULATION DETAILS

A. Separate Medium Calculations. As SM calculations have been performed earlier,¹⁸ we will only briefly describe the necessary equations. For a mobile dipolar solute with distribution function $\rho_s(\mathbf{r}, \mathbf{\Omega}; t)$, the expression for the position (\mathbf{r}), orientation ($\mathbf{\Omega}$), and time (t) dependent total fluctuating solvation energy is¹⁸

$$\begin{aligned} \delta E_{\text{total}}(\mathbf{r}, \mathbf{\Omega}, t) &= -k_B T \rho_s(\mathbf{r}, \mathbf{\Omega}, t) \left[\int d\mathbf{r}' d\mathbf{\Omega}' c_{\text{sd}}(\mathbf{r}, \mathbf{\Omega}; \mathbf{r}', \mathbf{\Omega}') \delta \rho_d(\mathbf{r}', \mathbf{\Omega}'; t) \right. \\ &\quad + \int d\mathbf{r}' d\mathbf{\Omega}' c_{\text{sp}}(\mathbf{r}, \mathbf{\Omega}; \mathbf{r}', \mathbf{\Omega}') \delta \rho_p(\mathbf{r}', \mathbf{\Omega}'; t) \\ &\quad \left. + \sum_{\alpha=1}^2 \int d\mathbf{r}' c_{\text{sa}}(\mathbf{r}, \mathbf{\Omega}; \mathbf{r}') \delta n_{\alpha}(\mathbf{r}', t) \right] \\ &= \delta E_{\text{sd}}(\mathbf{r}, \mathbf{\Omega}, t) + \delta E_{\text{sp}}(\mathbf{r}, \mathbf{\Omega}, t) + \delta E_{\text{si}}(\mathbf{r}, \mathbf{\Omega}, t) \end{aligned} \quad (1)$$

where $c_{\text{sd}}(\mathbf{r}, \mathbf{\Omega}; \mathbf{r}', \mathbf{\Omega}')$, $c_{\text{sa}}(\mathbf{r}, \mathbf{\Omega}; \mathbf{r}')$, and $c_{\text{sp}}(\mathbf{r}, \mathbf{\Omega}; \mathbf{r}', \mathbf{\Omega}')$ denote, respectively, the position and orientation dependent solute–dipolar ion (dipole–dipole), solute–ion (dipole–ion), and solute–dipolar solvent (dipole–dipole) direct correlation functions and α denotes the type of ions (cation and anion). $\delta \rho_d$ and δn_{α} represent the fluctuating IL dipolar and ion densities, and $\delta \rho_p$ represents the fluctuating polar solvent (added) density.¹⁸

The total (fluctuating) solvation energy autocorrelation function can then be expressed as

$$\begin{aligned} \langle \delta E_{\text{total}}(t) \delta E_{\text{total}}(t') \rangle &= \langle \delta E_{\text{sd}}(t) \delta E_{\text{sd}}(t') \rangle \\ &\quad + \langle \delta E_{\text{sp}}(t) \delta E_{\text{sp}}(t') \rangle + \langle \delta E_{\text{si}}(t) \delta E_{\text{si}}(t') \rangle, \end{aligned}$$

which may be rewritten as:

$$C_E(t) = C_{\text{sd}}(t) + C_{\text{si}}(t) + C_{\text{sp}}(t) \quad (2)$$

Equation 2 represents the correlation function made of three independent interaction contributions and has been derived after neglecting several cross-correlation terms.¹⁸ The normalized total solvation energy autocorrelation function then takes the following form:

$$\begin{aligned}
S_E(t) &= \frac{C_E(t)}{C_E(0)} \\
&= \frac{C_{sd}(t=0)S_{sd}(t)}{C_{sd}(t=0) + C_{si}(t=0) + C_{sp}(t=0)} \\
&\quad + \frac{C_{sp}(t=0)S_{sp}(t)}{C_{sd}(t=0) + C_{si}(t=0) + C_{sp}(t=0)} \\
&\quad + \frac{C_{si}(t=0)S_{si}(t)}{C_{sd}(t=0) + C_{si}(t=0) + C_{sp}(t=0)} \quad (3)
\end{aligned}$$

$$S_{sd}(t) = \frac{C_{sd}(t)}{C_{sd}(t=0)} = \frac{A \int_0^\infty dk k^2 S_{solute}^{10}(k, t) |c_{sd}^{10}(k)|^2 S_{IL}^{10}(k, t) + 2A \int_0^\infty dk k^2 S_{solute}^{11}(k, t) |c_{sd}^{11}(k)|^2 S_{IL}^{11}(k, t)}{A \int_0^\infty dk k^2 S_{solute}^{10}(k) |c_{sd}^{10}(k)|^2 S_{IL}^{10}(k) + 2A \int_0^\infty dk k^2 S_{solute}^{11}(k) |c_{sd}^{11}(k)|^2 S_{IL}^{11}(k)} \quad (4)$$

$$S_{sp}(t) = \frac{C_{sp}(t)}{C_{sp}(t=0)} = \frac{A \int_0^\infty dk k^2 S_{solute}^{10}(k, t) |c_{sp}^{10}(k)|^2 S_P^{10}(k, t) + 2A \int_0^\infty dk k^2 S_{solute}^{11}(k, t) |c_{sp}^{11}(k)|^2 S_P^{11}(k, t)}{A \int_0^\infty dk k^2 S_{solute}^{10}(k) |c_{sp}^{10}(k)|^2 S_P^{10}(k) + 2A \int_0^\infty dk k^2 S_{solute}^{11}(k) |c_{sp}^{11}(k)|^2 S_P^{11}(k)} \quad (5)$$

and

$$\begin{aligned}
S_{si}(t) &= \frac{C_{si}(t)}{C_{si}(t=0)} \\
&= \frac{B \sum_{\alpha, \beta} \sqrt{n_\alpha^0 n_\beta^0} \int_0^\infty dk k^2 S_{solute}^{10}(k, t) c_{s\alpha}^{10}(k) c_{s\beta}^{10}(-k) S_{\alpha\beta}^{ion}(k, t)}{B \sum_{\alpha, \beta} \sqrt{n_\alpha^0 n_\beta^0} \int_0^\infty dk k^2 S_{solute}^{10}(k) c_{s\alpha}^{10}(k) c_{s\beta}^{10}(-k) S_{\alpha\beta}^{ion}(k)} \quad (6)
\end{aligned}$$

where A is a prefactor given by $2\rho_d^0 k_B T / (2\pi)^2$.

Note $c_{sd}^{lm}(k)$ ($l, m = 1, 0$ or $1, 1$) in eq 4 and $c_{sp}^{lm}(k)$ ($l, m = 1, 0$ or $1, 1$) in eq 5 denote the Fourier transform of the (l, m) component of the static correlation functions between the solute and dipolar ions and between the solute and added dipolar solvent molecules, respectively. $c_{IL}^{lm}(k, t)$ and $c_P^{lm}(k, t)$ denote, respectively, the orientational dynamic structure factor for the IL and added dipolar solvent molecules. We have obtained these quantities earlier for neat ILs^{14–17,19–22} and (IL + polar solvent) binary mixtures¹⁸ by using the approximate method developed for common dipolar solvents.^{4,55–58} The relevant microscopic expressions are given below:

$$S_{IL}^{10}(k, t) = \frac{1}{4\pi 3Y} \left[1 - \frac{1}{\epsilon_L(k)} \right] L^{-1}[z + \Sigma_{10}(k, \omega)]^{-1} \quad (7)$$

and

$$S_{IL}^{11}(k, t) = \frac{1}{4\pi 3Y} [\epsilon_T(k) - 1] L^{-1}[z + \Sigma_{11}(k, \omega)]^{-1} \quad (8)$$

where $3Y = (4\pi/3k_B T)\mu^2\rho_d^0$ with μ and ρ_d^0 being the medium dipole moment and density. $[1 - \epsilon_L^{-1}(k)] = 3Yf_{110}^{-1}(k)$ and $[\epsilon_T(k) - 1] = 3Yf_{111}^{-1}(k)$ with $f_{ilm}(k) = 1 - (\rho_d^0/4\pi)(-1)^m c_{ilm}(k)$. These static direct correlation functions as well as $c_{sd}^{lm}(k)$ have been obtained from the MSA theory^{59,60} for (dipolar solute + dipolar solvent) binary mixtures in the limiting concentration of the dipolar solute by using the μ of neat systems. L^{-1} represents the Laplace inversion.

where $S_{sd}(t) = C_{sd}(t)/C_{sd}(t=0)$, $S_{sp}(t) = C_{sp}(t)/C_{sd}(t=0)$, and $S_{si}(t) = C_{si}(t)/C_{si}(t=0)$. Note eq 3 is the correct expression for the total normalized solvation energy correlation function.¹⁸ The total dynamic Stokes shift is then defined as²² $(C_E(t=0))^{1/2} = (C_{sd}(t=0))^{1/2} + (C_{si}(t=0))^{1/2} + (C_{sp}(t=0))^{1/2}$, which is equivalent to our earlier notation,¹⁸ $\Delta\nu_{tot}^t = \Delta\nu_{sd}^t + \Delta\nu_{si}^t + \Delta\nu_{sp}^t$. We will compare $\Delta\nu_{tot}^t$ thus obtained against experimental shifts^{23,41} measured at various mixture compositions.

The microscopic expressions for various components of the normalized total solvation energy autocorrelation function are given as follows¹⁸

$\Sigma_{lm}(k, \omega)$ denotes the wavenumber and frequency (ω) dependent generalized rate of the medium polarization relaxation and contains two frictional kernels: rotational ($\Gamma_R(k, z)$) and translational ($\Gamma_T(k, z)$). $\Gamma_R(k, z)$ is then connected to experimental $\epsilon(\omega)$ and $\Gamma_T(k, z)$ to solution viscosity (η) via approximate relations. References 15–17 provide the details regarding calculation of these quantities for neat ILs and ref 18 for (IL + polar solvent) binary mixtures. Note experimental $\epsilon(\omega)$ values for neat ILs and neat dipolar solvents are required for SM calculations, whereas the same for (IL + polar solvent) binary mixtures are needed for EM calculations. Likewise, $S_P^{lm}(k, t)$ has been determined by using the experimental $\epsilon(\omega)$ of neat dipolar solvents. $S_{solute}^{lm}(k, t)$, the solute dynamic structure factor, has been obtained by using the relation^{4,14–22}

$$S_{solute}^{lm}(k, t) = \frac{1}{4\pi} \exp[-(l(l+1)D_R^s + k^2 D_T^s)t] \quad (9)$$

where D_R^s and D_T^s are the rotational and translational diffusion coefficients of the solute, determined via hydrodynamics using the stick boundary condition and η .^{23,45}

The prefactor of eq 6 is $B = 2(k_B T/2\pi)^2$. $c_{s\alpha}^{10}(k)$ denotes the longitudinal component of the wavenumber dependent static structural correlations between the dipolar solute and an ion of type α , given by

$$c_{s\alpha}^{10}(k) = -\sqrt{\frac{4\pi}{3}} \left(\frac{4\pi i \mu_1 q_\alpha}{k_B T \epsilon_0 k} \right) \frac{\sin(kr_c)}{kr_c} \quad (10)$$

where μ_1 is the excited state dipole moment of the dissolved dipolar solute, q_α the charge on the α th type ion, and r_c the distance of the closest approach between the solute dipole and the ionic species. The diffusive form for $S_{\alpha\beta}^{ion}(k, t)$ (eq 6) has been used and $S_{\alpha\alpha}(k)$ approximated by the Percus–Yevick (P–Y) solution.⁶¹ For the calculations of $S_{\alpha\beta}^{ion}(k, t)$, expressions derived elsewhere^{62,63} have been used.

B. Effective Medium Calculations. The EM approach considers dipolar ions and the added dipolar solvent molecules

jointly as a united effective dipolar entity characterized by an effective dipole moment determined via MSA theory using experimental ϵ_0 and an effective dipolar diameter defined as

$$\sigma_d = [x_{\text{IL}}\sigma_d^3 + (1 - x_{\text{IL}})\sigma_p^3]^{1/3} \quad (11)$$

where x_{IL} denotes the IL mole fraction in the mixture, σ_d the diameter of the IL dipolar cation, and σ_p the diameter of the added dipolar solvent molecule. The effective dipolar molar mass is also calculated as a mole fraction weighted sum of the dipolar component masses. The total shift in EM calculation is considered as

$$\Delta\nu_{\text{tot}}^{\text{eff}} = \Delta\nu_{\text{sd}}^{\text{eff}} + \Delta\nu_{\text{si}}^{\text{eff}} \quad (12)$$

and the normalized solvation energy autocorrelation function as

$$\begin{aligned} S_E^{\text{eff}}(t) &= \frac{C_E^{\text{eff}}(t)}{C_E^{\text{eff}}(0)} \\ &= \frac{C_{\text{sd}}^{\text{eff}}(t=0)S_{\text{sd}}^{\text{eff}}(t)}{C_{\text{sd}}^{\text{eff}}(t=0) + C_{\text{si}}^{\text{eff}}(t=0)} \\ &\quad + \frac{C_{\text{si}}^{\text{eff}}(t=0)S_{\text{si}}^{\text{eff}}(t)}{C_{\text{sd}}^{\text{eff}}(t=0) + C_{\text{si}}^{\text{eff}}(t=0)} \end{aligned} \quad (13)$$

Subsequently, $\Delta\nu_{\text{tot}}^{\text{eff}}$ and $S_{\text{sx}}^{\text{eff}}(t)$ (x being d or i) are obtained following the method described for SM calculations using the experimental dielectric relaxation data for (IL + polar solvent) binary mixtures. In addition, x_{IL} dependent static orientational correlations have been obtained by using the effective medium μ at that composition determined from experimental x_{IL} dependent ϵ_0 by using the corresponding MSA relation. Other physical parameters necessary for calculations are taken from experiments and summarized in Tables S1 and S2 in the Supporting Information.

III. RESULTS AND DISCUSSION

A. Composition Dependent Dynamic Stokes Shift: Comparison between Theory and Experiments. Figure 1 presents the composition dependent dynamic Stokes shifts predicted from EM and SM calculations for C153 in ([Bmim][BF₄] + CH₃CN) and ([Bmim][BF₄] + H₂O) binary mixtures at 298 K and compares them with those from (FLUPS + TCSPC) measurements reported, respectively, by Liang et al.⁴⁵ and Zhang et al.²³ For EM calculations of x_{IL} dependent dynamic Stokes shift magnitudes and solvation response functions, we have used experimental $\epsilon(\omega)$ reported in ref 23 for ([Bmim][BF₄] + H₂O) mixtures and those in ref 46 for ([Bmim][BF₄] + CH₃CN) mixtures. The dynamic shift and response function for neat IL ($x_{\text{IL}} = 1$) have been obtained via SM calculations using $\epsilon(\omega)$ for neat IL from ref 23. For SM calculations of x_{IL} dependent dynamic shifts and response functions, $\epsilon(\omega)$ reported in ref 23 for neat [Bmim][BF₄], ref 46 for CH₃CN, and ref 64 for H₂O have been used. In addition, the liquid phase dipole moment (2.85 D)^{65,66} has been used for water while carrying out SM calculations for ([Bmim][BF₄] + H₂O) binary mixtures. Strikingly, EM predictions are in semiquantitative agreement with those from measurements,^{23,45} reproducing well the experimentally observed near-insensitivity to the mole fraction of the dynamic Stokes shift in these binary mixtures. SM calculations, in contrast, predict pronounced nonideal composition dependence, showing a strong deviation from the experimental trend.^{23,45} The differing sensitivity to

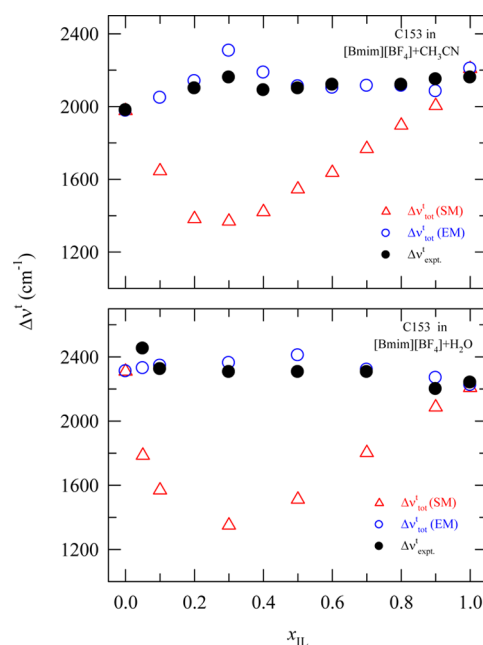


Figure 1. Comparison of composition dependent dynamic Stokes shifts between theory and experiments for C153 in ([Bmim][BF₄] + CH₃CN) and ([Bmim][BF₄] + H₂O) binary mixtures. Experimental results are denoted by filled circles. Open circles denote the effective medium (EM) predictions, and open triangles represent those from separate medium (SM) calculations. Note, while the calculations are done at ~298 K, the experimental results correspond to (FLUPS + TCSPC) measurements at ~293 K.

mixture composition of EM and SM approaches in predicting dynamic shifts arises from the use of effective dipole moment and dipole size in one case and individual values for the neat components in the other. Below we elaborate on this aspect.

Figure 2 examines the composition dependence of the various interaction contributions to the total calculated shifts from the EM and SM approaches for C153 in ([Bmim][BF₄] + CH₃CN) mixtures. Similar analyses for aqueous mixtures of [Bmim][BF₄] are presented in Figure S3 (Supporting Information). Calculated results displayed in the upper panel suggest that EM calculations predict a decrease of the solute-medium dipolar contribution ($\Delta\nu_{\text{sd}}^{\text{t}}$) with an increase of IL mole fraction (x_{IL}) in the mixture. This is compensated by the equal amount of increase of the ion–dipole interaction contribution ($\Delta\nu_{\text{si}}^{\text{t}}$), forcing the calculated total shift ($\Delta\nu_{\text{tot}}^{\text{t}}$) to remain insensitive to x_{IL} . Gradual increase of x_{IL} enhances the solute–ion static correlations (c_{sd}^{10}) due to the subsequent decrease in ϵ_0 of the mixture (see eq 10). This and the increase of ion density with x_{IL} (see Table S1, Supporting Information) which is present as a multiplicative factor in the working expression (see the denominator of eq 6) are jointly responsible for the predicted increase of $\Delta\nu_{\text{si}}^{\text{t}}$ with IL concentration. Interestingly, data in Table S1 (Supporting Information) also indicate that the effective dipole number density ($\rho_{\text{N}}^{\text{d}}$) decreases with IL mole fraction as the mass density (ρ) increases. Such a decrease in $\rho_{\text{N}}^{\text{d}}$ with x_{IL} reduces the solute–IL dipole–dipole static correlations, $c_{\text{sd}}^{10}(k)$. This is shown in Figure S4 (Supporting Information). Consequently, $\Delta\nu_{\text{sd}}^{\text{t}}$ calculated via the denominator of eq 4, decreases as x_{IL} increases in the mixture. Similarly, the x_{IL} dependence of dynamic shifts in ([Bmim][BF₄] + H₂O) mixtures predicted by EM calculations can be explained. Note the use of the liquid

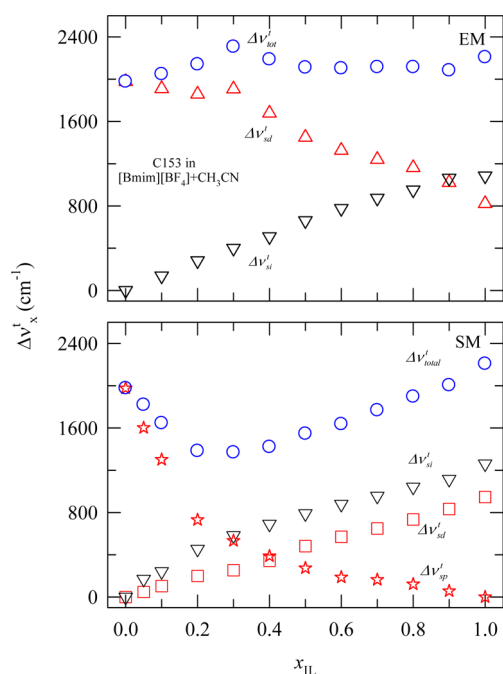


Figure 2. Composition dependence of the various interaction contributions to the total calculated shifts from the EM and SM calculations for C153 in ([Bmim][BF₄] + CH₃CN) mixtures. The same for the aqueous mixture is shown in Figure S3 (Supporting Information). Symbol representations are indicated in each of the panels.

phase dipole moment for water^{65,66} has produced a total shift of $\sim 2000 \text{ cm}^{-1}$ for C153 in ([Bmim][BF₄] + H₂O) mixtures at $x_{\text{IL}} \rightarrow 0$. Numerical results shown in the lower panel of Figure 2 suggest that SM calculations predict a different x_{IL} dependence for the dipolar contributions, $\Delta\nu_{\text{sd}}^{\text{t}}$ and $\Delta\nu_{\text{sp}}^{\text{t}}$. For $\Delta\nu_{\text{sd}}^{\text{t}}$ the composition dependence remains the same as predicted by the EM calculations. The near-linear increase of $\Delta\nu_{\text{sd}}^{\text{t}}$ and $\Delta\nu_{\text{si}}^{\text{t}}$ follows the x_{IL} dependence of the IL dipolar and ion number densities, shown in Figure S5 (Supporting Information). The number density for the added dipolar solvent molecules, however, exhibits a nonlinear mixture composition dependence (see Figure S5, Supporting Information). Note these densities are mole fraction weighted densities at each composition of these binary mixtures. This nonlinearity of density with x_{IL} produces the nonlinear composition dependence for $\Delta\nu_{\text{sp}}^{\text{t}}$ predicted by SM calculations. A nonlinear decrease of $\Delta\nu_{\text{sp}}^{\text{t}}$ and near-linear increase of $\Delta\nu_{\text{sd}}^{\text{t}}$ then combines to render a strong nonideal composition dependence of the total shift, $\Delta\nu_{\text{tot}}^{\text{t}}$ predicted by the SM approach for these binary mixtures.

We next examine what connects our EM calculations to the experimental observation²³ that the volume fraction, rather than the mole fraction, is a better descriptor for the spectral shifts in (IL + polar solvent) binary mixtures. A link between the composition dependent effective number densities (both for dipolar and ionic specie) and the IL volume is the key here. Equations 11 and 12 in Appendix 1 (Supporting Information) provide an approximate connection between the effective number densities to the mole fraction (x_{IL}) weighted volumes of IL and added polar solvent molecules. Since the IL volume ($\sigma_{[\text{Bmim}]^+} = 6.78 \text{ \AA}$ and $\sigma_{[\text{BF}_4]^-} = 4.58 \text{ \AA}$)¹⁵ is much larger than that of the added polar solvent molecules ($\sigma_{\text{H}_2\text{O}} = 2.8 \text{ \AA}$ ⁶⁷ and $\sigma_{\text{CH}_3\text{CN}} = 4.5 \text{ \AA}$)⁶⁸, the effects of the IL volume on number

density dominate. In EM calculations, this translates to a much larger solute–IL dipolar interaction contribution to the calculated shift than that obtained via employing the mole fraction weighted densities (SM calculations). This is depicted in Figure S6 (Supporting Information) which shows that dipolar contributions predicted by the EM approach in the $0.1 \leq x_{\text{IL}} \leq 0.8$ region substantially outweigh the combined dipolar contributions ($\Delta\nu_{\text{sd}}^{\text{t}} + \Delta\nu_{\text{sp}}^{\text{t}}$) from SM calculations. The effect of IL volume via number density on solute–IL interaction is probably the reason for the spectral shifts in (IL + polar solvent) mixtures showing a nearly linear dependence on IL volume fraction.²³

B. Composition Dependent Stokes Shift Dynamics: Comparison between Theory and Experiments. For comparison, the following normalized solvation response function has been constructed

$$S_{\text{ss}}(t) = (1 - 0.1x_{\text{IL}})[x_{\text{IL}}S_{\text{sd}}(t) + (1 - x_{\text{IL}})S_{\text{sp}}(t)] + 0.1x_{\text{IL}}S_{\text{si}}(t) \quad (14)$$

where S_{sd} , S_{sp} , and S_{si} are obtained from eqs 4, 5, and 6, respectively. Equation 14 is for SM prediction which correctly reduces to the corresponding neat liquid expression. For EM, the effective dipole–dipole interaction contribution term absorbs S_{sp} , producing $S_{\text{ss}}(t) = (1 - 0.1x_{\text{IL}})S_{\text{sd}}(t) + 0.1x_{\text{IL}}S_{\text{si}}(t)$.

Note $S_{\text{ss}}(t)$ for neat ILs considers^{15–22} only 10% contribution from $S_{\text{si}}(t)$ which, for these binary mixtures, has become x_{IL} dependent here. Such a small contribution from ion dynamics in our theory^{15–22} was motivated by experimental results on Stokes shift dynamics of electrolyte solutions in polar solvents.⁶⁹ Note the factors that are important for bringing theory and experiments closer are the proper descriptions of static solute–solvent and solvent–solvent correlations and inclusion of natural dynamics of these complex mixtures. The collective nature of dynamic Stokes shift experiments renders secondary importance to static short-range correlations, and hence, a qualitatively correct description of them may suffice. Information regarding natural dynamics is incorporated via the use of experimental $\epsilon(\omega)$ measured over a broad frequency range. These factors lead to semiquantitative prediction of experimental solvation response functions.

(i). ([Bmim][BF₄] + CH₃CN) Binary Mixtures. Figure 3 presents calculated solvation response functions at 298 K for three representative compositions of ([Bmim][BF₄] + CH₃CN) binary mixtures and compares them with the corresponding C153/(FLUPS + TCSPC) measurements by Liang et al.⁴⁵ Note while EM predictions are made using experimental $\epsilon(\omega)$ reported in ref 46 for mixture compositions $0 < x_{\text{IL}} < 1$, SM calculations employed $\epsilon(\omega)$ for neat IL from ref 23 (that is, $\epsilon(\omega)$ at $x_{\text{IL}} = 1$) and for neat CH₃CN from ref 46 ($x_{\text{IL}} = 0$). Calculated (using $\epsilon(\omega)$ from ref 23) and experimental response functions for pure [Bmim][BF₄] are also presented in each panel to show the effects of polar solvent on IL dynamics. The following aspects are to be noted. First, both EM and SM calculations predict acceleration of average solvation rate upon addition of polar solvent into IL and can well reproduce the experimentally observed slow long-time dynamics at these compositions.⁴⁵ Second, the early time dynamics predicted by the SM calculations is faster than that observed in experiments⁴⁵ for all these mixture compositions, while the opposite is predicted by EM calculations. Third, the difference in solvation rates between the neat and mixtures at the initial phase is larger in SM predictions than that in

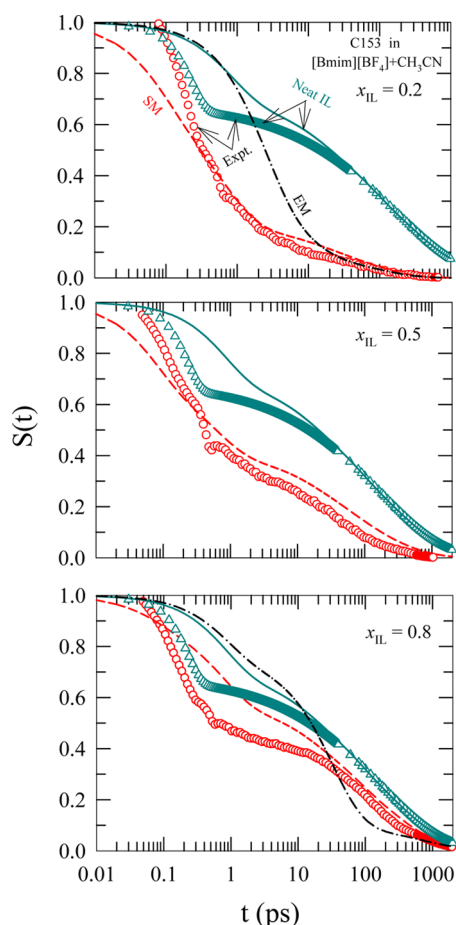


Figure 3. Comparison between the calculated and measured solvation response functions for C153 in a ([Bmim][BF₄] + CH₃CN) mixture at three representative IL mole fractions. Both EM and SM predictions (dashed-dot and dashed lines, respectively) are shown for each of these IL mole fractions. Predicted response functions for neat IL are denoted by the solid line. Circles and triangles represent the (FLUPS + TCSPC) data, respectively, for the (IL + CH₃CN) mixture and the neat IL. Representations remain the same for each panel. The EM prediction at $x_{\text{IL}} = 0.5$ has not been made because of the nonavailability of experimental $\epsilon(\omega)$ at this mixture composition. Note, while the calculations are done at ~ 298 K, the experimental results correspond to (FLUPS + TCSPC) measurements at ~ 293 K.

experiments.⁴⁵ Fourth, both EM and SM calculations can reproduce only weakly the strong bimodal character of the measured response, which increasingly softens upon successive dilution of IL with polar solvent. Fifth, the predicted short-time SM dynamics appears to be faster than in experiments and this is so even without including the high frequency DR contributions in these calculations. This is because the experimental $\epsilon(\omega)$ values²³ used here for these mixtures report ϵ_{∞} values much larger than the square of the refractive index (n_{D}^2) of neat [Bmim][BF₄] ($n_{\text{D}}^2 \approx 2.02$)^{70,71} and CH₃CN ($n_{\text{D}}^2 \approx 1.8$).^{46,72}

Table S7 (Supporting Information) summarizes the amplitudes (a_i), time constants (τ_i), and stretching exponents (β) obtained from fits to the calculated and measured response functions.⁴⁵ Note fit parameters only from SM calculations are shown in this table, as these predictions are in better agreement with experiments⁴⁵ than EM calculations. We would also like to mention here that, in comparison to the experimental response functions⁴⁵ being well-described by a sum of a Gaussian and

three exponentials (that is, $S(t) = f_{\text{G}} \times \exp[-(\omega_{\text{G}}t)^2/2] + (1 - f_{\text{G}}) \sum_{i=1}^3 b_i \exp(-t/\tau_i)$, with $\sum_{i=1}^3 b_i = 1$) for ([Bmim][BF₄] + CH₃CN) binary mixtures at all compositions studied, the SM predictions at $x_{\text{IL}} \geq 0.4$ were found to fit well to both a sum of four exponentials and a sum of an exponential and a stretched exponential (that is, $S_{\text{ss}}(t) = a_1 \exp(-t/\tau_1) + a_2 \exp(-t/\tau_2)^{\beta}$, with β as the stretching exponent and $a_1 + a_2 = 1$). At $x_{\text{IL}} < 0.4$, a sum of three or four exponentials could describe the predicted response functions and use of a stretched exponential in this regime along with an exponential or a sum of exponentials was found to worsen the fit. These features are shown in Figure S8 (Supporting Information). Parameters from four-exponential fits are shown in Table S7 (Supporting Information) only to facilitate comparison between theory and experiments, although parameters obtained from other economical fits are also tabulated. In addition, at no stage did we find emergence of a Gaussian ultrafast component in the predicted dynamics because the experimental $\epsilon(\omega)$ used in these calculations did not include the contributions from the high frequency collective intermolecular modes.

A closer inspection of the data summarized in Table S7 (Supporting Information) reflects the following facts. At $x_{\text{IL}} = 0.05$, the average solvation time ($\langle \tau_{\text{solv}} \rangle = \int_0^{\infty} dt S(t)$) is ~ 5 times larger than that in neat CH₃CN ($\langle \tau_{\text{solv}} \rangle_{\text{acn}} = 0.26$ ps),^{9,45} although the amplitude-weighted fast time constants ($a_1 \tau_1$) remain nearly the same. Interestingly, $a_2 \tau_2$ is ~ 4 times larger in the binary mixture than that in neat CH₃CN. This can be explained by recalling that the slower component of the bimodal experimental $\epsilon(\omega)$ at this composition relaxes with a time constant ~ 5 times larger than that for neat CH₃CN.⁴⁵ In addition, a slow time constant appears in DR measurements at $x_{\text{IL}} \rightarrow 0$, which has been attributed to ion-pair relaxation.⁴⁶ Therefore, the overall slowing down of the neat CH₃CN dynamics upon addition of IL may be connected to the slow Cole–Cole component in $\epsilon(\omega)$ with ion-pair relaxation and ion translation in the (IL + CH₃CN) mixture. Similar arguments may also be used for interpreting the calculated dynamics at $x_{\text{IL}} = 0.1$. These characteristics at very low IL concentrations should be cross-checked via further experiments.

At higher IL concentrations ($x_{\text{IL}} \geq 0.2$) for which (FLUPS + TCSPC) measurements are available,⁴⁵ SM calculations compare favorably with experiments.⁴⁵ Particularly, the slowest of the four time constants, which is in the ~ 0.1 – 1 ns range, matches very well with those from measurements. Consequently, the predicted average solvation and slow times ($\langle \tau_{\text{solv}} \rangle$ and $\langle \tau_{\text{s}} \rangle$, respectively) are in semiquantitative agreement with those from measurements.⁴⁵ This is shown in Figure 4. In the same figure, the x_{IL} dependent ultrafast time constants ($\langle \tau_{\text{f}} \rangle$) are also compared. Note, while the experimental τ_{f} remains nearly insensitive to mixture composition and agrees well with the SM predictions up to $x_{\text{IL}} \leq 0.5$, the predicted values at $x_{\text{IL}} > 0.5$ appear to show a linear increase with x_{IL} . This is an incorrect prediction arising from the use of experimental $\epsilon(\omega)$ as input which does not include the high frequency contribution to its full dispersion.

Next we explore how inclusion of the high frequency contribution to $\epsilon(\omega)$ alters EM predictions of solvation response and subsequent comparisons with experiments at various IL mole fractions in ([Bmim][BF₄] + CH₃CN) binary mixtures. The high frequency contribution is incorporated in the available experimental $\epsilon(\omega)$ ⁴⁶ via assigning the undetected dispersion, $\epsilon_{\infty} - n_{\text{D}}^2$, to a collective intermolecular mode at 30 cm^{-1} . Note this is purely a model calculation where assignment

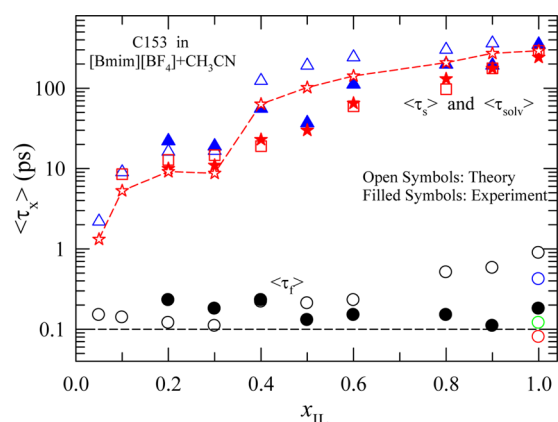


Figure 4. Comparison of various measures of IL mole fraction dependent average times between theory and experiments for C153 in a ([Bmim][BF₄] + CH₃CN) mixture. Open triangles represent average slow times ($\langle \tau_s \rangle$), open stars the average solvation times ($\langle \tau_{\text{solv}} \rangle$), and open circles the average ultrafast time ($\langle \tau_f \rangle$) from SM calculations. Open squares mark the $\langle \tau_{\text{solv}} \rangle$ from EM calculations. $\langle \tau_s \rangle$, $\langle \tau_{\text{solv}} \rangle$, and $\langle \tau_f \rangle$ from (FLUPS + TCSPC) measurements are represented by the filled triangles, filled stars, and filled circles, respectively. At $x_{\text{IL}} = 1.0$ (neat IL), blue and red circles represent calculated times in the absence and presence of high frequency intermolecular collective mode contribution (ref 22) and the green circle denotes the prediction reported in ref 15. Calculated times correspond to ~ 298 K, measurements to ~ 293 K.

of the entire missing dispersion to this particular mode may not be a proper description of the collective dynamics in these mixtures at this frequency regime, but several simulation and experimental studies have confirmed existence of this mode in various neat ILs. We have employed the methodology described in our earlier study²² for systematic incorporation of this high frequency contribution in $\epsilon(\omega)$ after setting $n_D^2 = 2$ at all mole fractions and using x_{IL} dependent ϵ_∞ from experiments. Figure 5 compares experimental response functions with EM predictions in the absence and presence of high frequency contributions at three representative IL mole fractions. Evidently, proposed coupling of the 30 cm^{-1} intermolecular mode leads to a substantial acceleration of the rate at the early and middle stages of the time-dependent solvation, producing an ultrafast component much sharper than those observed in experiments. In fact, these calculations predict, upon inclusion of a high frequency contribution in $\epsilon(\omega)$, a nearly x_{IL} independent ultrafast time scale in the sub-100 fs regime.²² Parameters obtained from multiexponential fits to the calculated response functions summarized in Table S9 (Supporting Information) demonstrate this. A similar observation has also been made with SM calculations (results not shown) when the high frequency contributions are incorporated in the DR of respective neat solvents. Another aspect to be noticed is that, even though the EM calculations without the high frequency contribution appear different from and slower than the experimental response functions,⁴⁵ $\langle \tau_{\text{solv}} \rangle$ obtained from them agree well with those from experiments (shown as squares in Figure 4). In fact, $\langle \tau_{\text{solv}} \rangle$ from EM calculations in Figure 4 appear to be closer to experimental values than those from SM calculations, although the time profiles of the experimental solvation response functions are better described by the SM approach. This observation therefore suggests that both of the approaches can successfully predict the average rate of solvation in these mixtures, although none of the approaches

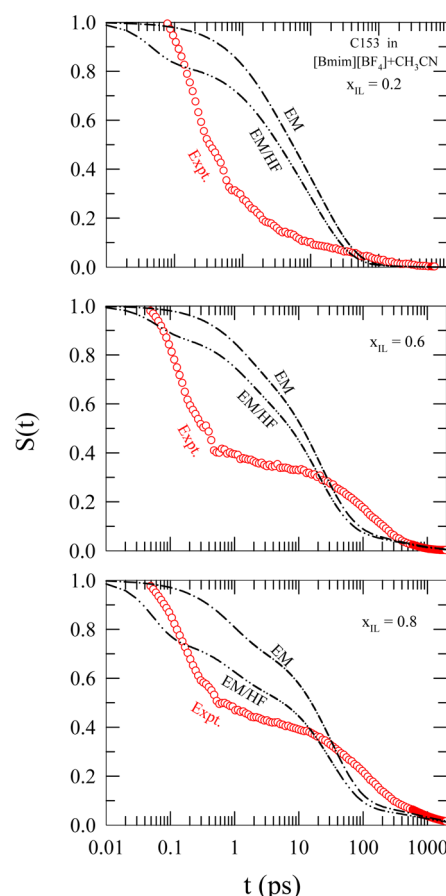


Figure 5. Effects of collective intermolecular solvent modes on solvation response predicted by EM calculations for C153 in a ([Bmim][BF₄] + CH₃CN) mixture at three representative IL mole fractions. The impact of the collective solvent mode enters via $\epsilon(\omega)$ used as input in the present calculations. See text for details. “EM/HF” represents predicted solvation response functions from EM calculations after incorporating the contribution in $\epsilon(\omega)$ from the high frequency (30 cm^{-1}) intermolecular mode. This frequency has been kept fixed for calculations at all mixture compositions. “EM” denotes predictions in the absence of this high frequency mode. Circles represent (FLUPS + TCSPC) data at these IL mole fractions.

can quantitatively reproduce the measured response functions over the entire time domain. Measurements of $\epsilon(\omega)$ with broader frequency coverage for these mixtures are therefore required for more accurate predictions of experimental Stokes shift dynamics by this semimolecular theory.

(ii). ([Bmim][BF₄] + H₂O) Binary Mixtures. Figure 6 compares the EM and SM predicted solvation response functions with the corresponding (FLUPS + TCSPC) measurements²³ at three representative x_{IL} . The EM calculations are done at 298 K by using experimental $\epsilon(\omega)$ for ([Bmim][BF₄] + H₂O) binary mixtures,²³ and the SM predictions by using those for neat [Bmim][BF₄]²³ and H₂O.⁶⁴ Calculated and experimental response functions for neat [Bmim][BF₄] are also shown in these panels to highlight the effects of water on neat IL dynamics. As observed for ([Bmim][BF₄] + CH₃CN) binary mixtures, the EM predictions are slower than both SM predictions and experimental response functions for most of the time except at the late to very late stage of solvation, with the difference being wider at lower x_{IL} . In addition, SM calculations predict larger effects, particularly at low x_{IL} , of water on neat IL dynamics than that observed in

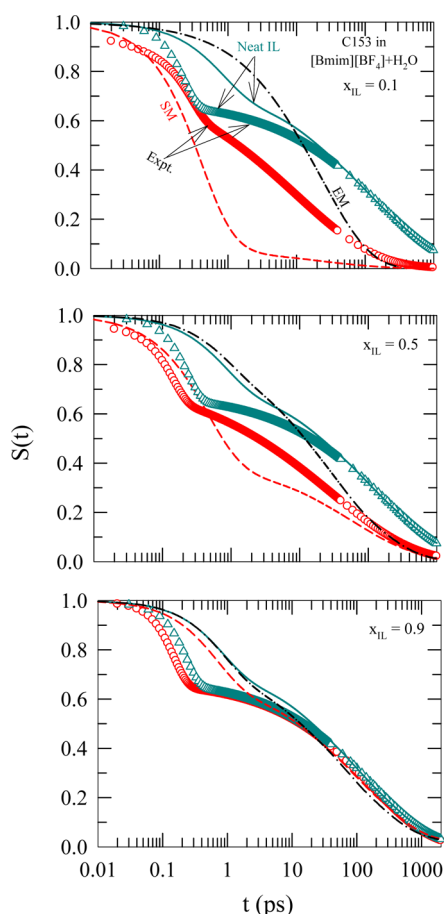


Figure 6. Comparison between the calculated and measured solvation response functions for C153 in a ([Bmim][BF₄] + H₂O) mixture at three representative IL mole fractions. While lines in these panels represent calculations at ~ 298 K, the symbols denote (FLUPS + TCSPC) measurements at ~ 293 K. Other representations remain the same as in Figure 3.

experiments. This becomes more obvious when we compare the predicted ratios of $\langle \tau_{\text{solv}} \rangle$ between the neat IL and a given x_{IL} with those from measurements. For example, the fit parameters summarized in Table S10 (Supporting Information) indicate that the ratio $(\langle \tau_{\text{solv}} \rangle^{\text{IL}} / \langle \tau_{\text{solv}} \rangle^{\text{mix}})$ at $x_{\text{IL}} = 0.05$ is ~ 71 from SM calculations, which is nearly 5 times larger than the ratio between the corresponding experimental times. This factor of ~ 5 at $x_{\text{IL}} = 0.05$ reduces to ~ 0.9 at $x_{\text{IL}} = 0.9$, suggesting better performance of the theory for IL rich mixtures. However, relevant experiments report that the Stokes shift dynamics at this low x_{IL} is too fast to be accurately measured.²³ Note that the parameters shown in Table S10 (Supporting Information) have been obtained from fitting the SM predictions to a sum of fast exponential and stretched exponential functions of time at all IL mole fractions. This is different from experiments where multiexponential or a combination of Gaussian and stretched exponential functions were found to adequately describe the measured response functions. Data in Table S10 (Supporting Information) also reflect that the ultrafast time constant which is in the ~ 100 – 300 fs range in experiments is predicted to be much slower (~ 500 – 900 fs) in these calculations. As before, we ascribe this poor agreement to the noninclusion of high frequency contribution to DR in our calculations.

Figure 7 compares x_{IL} dependent various average times ($\langle \tau_{\text{f}} \rangle$, $\langle \tau_{\text{s}} \rangle$, and $\langle \tau_{\text{solv}} \rangle$) from SM calculations and experiments for

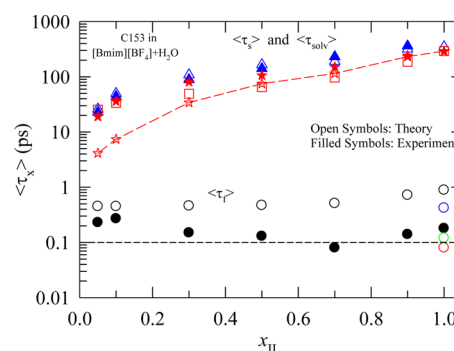


Figure 7. Comparison of various measures of IL mole fraction dependent average times between theory and experiments for C153 in a ([Bmim][BF₄] + H₂O) mixture. Representations remain the same as in Figure 4.

([Bmim][BF₄] + H₂O) binary mixtures. Note that, while predicted $\langle \tau_{\text{s}} \rangle$ values are in semiquantitative agreement with those from experiments for the entire mole fraction range studied,²³ such an agreement for $\langle \tau_{\text{solv}} \rangle$ occurs for solutions with $x_{\text{IL}} \geq 0.5$. The large difference between the predicted and experimental amplitudes of the slow stretched component at $x_{\text{IL}} < 0.5$ (see Table S10, Supporting Information) is the reason for the observed disagreement. As before, $\langle \tau_{\text{solv}} \rangle$ from EM calculations (squares) agree well with experiments over the entire x_{IL} range. This is because of the competitive effects on $\langle \tau_{\text{solv}} \rangle$ of the slow component amplitude and the stretching exponent (β) value associated with it (Table S11, Supporting Information). The absence of this compensating effect in $\langle \tau_{\text{s}} \rangle$ is the reason for EM predictions not showing a similar level of agreement with those from measurements. Figure 7 also indicates that $\langle \tau_{\text{f}} \rangle$ predicted by SM calculations are uniformly larger than those from measurements,²³ and show a different x_{IL} dependence. This may be linked to the absence of high frequency intermolecular contribution in $\epsilon(\omega)$ ²³ used in our SM calculations.

The importance of the high frequency intermolecular contribution in $\epsilon(\omega)$ ²³ for Stokes shift dynamics is further highlighted in Figure 8 where predicted response functions from EM calculations in the absence and presence of high frequency intermolecular contribution to $\epsilon(\omega)$ at three representative x_{IL} of ([Bmim][BF₄] + H₂O) mixtures are compared with experiments. Corresponding fit parameters summarized in Table S11 (Supporting Information) clearly indicate that the experimentally observed ultrafast time scale in the ~ 30 – 300 fs range can be recovered only after incorporating the high frequency IL intermolecular mode contribution to $\epsilon(\omega)$. As discussed earlier,²² the missing dispersion, $\epsilon_{\infty} - n_{\text{D}}^2$, is attributed to an IL intermolecular mode at 30 cm^{-1} with ϵ_{∞} taken from x_{IL} dependent measurements and n_{D}^2 fixed at 2. Note the inclusion of this intermolecular mode not only generates an ultrafast time scale of ~ 50 – 200 fs but reduces also β values which affects both $\langle \tau_{\text{solv}} \rangle$ and $\langle \tau_{\text{s}} \rangle$. Given that the Stokes shift dynamics of an excited dipolar probe in neat water is characterized by an ultrafast component with a time constant of ~ 60 fs and that of neat IL with ~ 200 fs, the above range predicted by EM calculations for the ([Bmim][BF₄] + H₂O) binary mixture is expected and reflective of the role played by the collective solvent intermolecular modes in dictating the

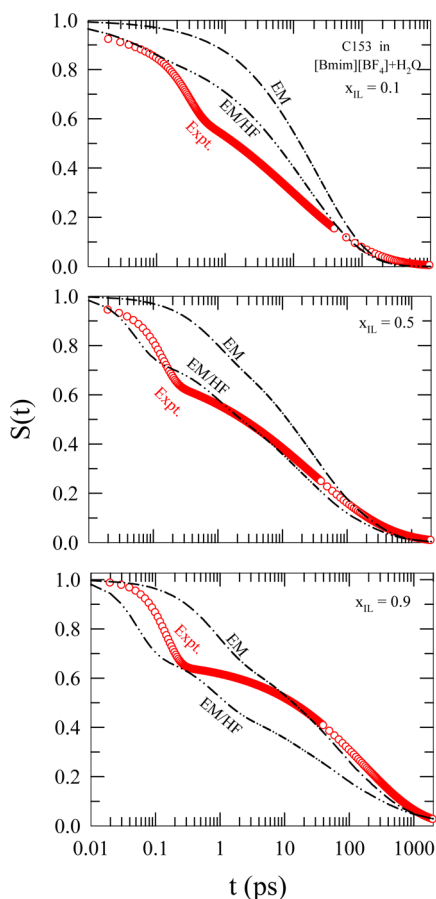


Figure 8. Effects of collective intermolecular solvent modes on solvation response predicted by EM calculations for C153 in a ([Bmim][BF₄] + H₂O) mixture at three representative IL mole fractions. The frequency of the collective solvent mode is fixed at 30 cm⁻¹ for all compositions considered. Other representations remain the same as in Figure 5.

ultrafast polar solvation energy relaxation in such aqueous mixtures.

We next highlight the variations in SM-predicted response functions obtained by using different experimental $\epsilon(\omega)$ for [Bmim][BF₄], and the subsequent agreement between calculations and (FLUPS + TCSPC) measurements. For example, earlier DR measurements of neat [Bmim][BF₄] at ~ 298 K with a frequency coverage of 0.2–89 GHz represented $\epsilon(\omega)$ as a combination of a Cole–Cole and a Debye (CC + D) process with a fast (Debye) time constant of ~ 600 fs and $\epsilon_\infty = 2.57$.⁷³ Later measurements of this IL with the same frequency coverage at this temperature have expressed $\epsilon(\omega)$ as a sum of four Debye processes with a fast time constant of ~ 1 ps and $\epsilon_\infty = 3.34$.⁴⁶ Also, values of ϵ_0 and the slowest time constant vary between measurements. These variations are likely to impact the predicted response functions. Figure S12 (Supporting Information) explores such effects via comparing SM predicted response functions using these different experimental $\epsilon(\omega)$ with the experimental data²³ at three x_{IL} values for the ([Bmim]-[BF₄] + H₂O) mixture. As evidenced in this figure, although both $\epsilon(\omega)$ can reproduce qualitatively the bimodal character of the measured response functions, the bimodality becomes more distinct when a (CC + D) description of $\epsilon(\omega)$ is used (particularly at higher x_{IL}) due to the presence of a faster Debye time constant and a stretching exponent, α . Another related

issue we address is how predicted response functions vary if different water dipole moments (gas and liquid phases) are used in calculations. We have already found that the magnitude of the dynamic Stokes shift increases when a larger dipole moment (liquid phase) for water is used in our calculations but argued that the rate of the solvation energy relaxation should remain unaltered within such a linearized theory (that is, time dependent solvation energy linear to fluctuating solvent density, $\delta\rho(t)$) where time dependence in static correlations (solute–solvent and solvent–solvent) is completely ignored. SM-predicted solvation response functions at two representative x_{IL} shown in Figure S13 (Supporting Information) indeed suggest that different water dipole moments (1.8 and 2.8 D) do not lead to any difference in the calculated decay rates. When the viscosity (η) dependence of the slow times ($\langle\tau_s\rangle$) was explored, we found $\langle\tau_s\rangle \propto \eta^p$ with $p \approx 0.6$ for ([Bmim][BF₄] + H₂O) mixtures (see upper panel of Figure S14, Supporting Information), which agrees well with the relevant experiments.²³ Similar analyses for ([Bmim][BF₄] + CH₃CN) mixtures produce $p \approx 0.9$ if the calculated $\langle\tau_s\rangle$ for all x_{IL} studied are considered in the correlation (see lower panel, Figure S14, Supporting Information). However, like in experiments,⁴⁵ if one considers $\langle\tau_s\rangle$ in the $x_{\text{IL}} = 0.2$ –1.0 range, one obtains $p \approx 0.8$, which is much closer to that ($p \approx 0.7$) reported by the corresponding measurements.⁴⁵

Subsequently, we cross-check whether the calculated average solvation times show, like in experiments, a deviation from dielectric continuum prediction of linear dependence when plotted as a function of inverse conductivity, σ^{-1} .²³ Figure 9 presents such an analysis where the calculated x_{IL} dependent average solvation times ($\langle\tau_{\text{ss}}\rangle$), the average times from dipolar and ion components ($\langle\tau_{\text{sd}}\rangle$ and $\langle\tau_{\text{si}}\rangle$, respectively), and the measured average solvation times ($\langle\tau_{\text{solv}}\rangle$) are shown in the upper panel as a function of x_{IL} dependent measured σ^{-1} for ([Bmim][BF₄] + H₂O) mixtures. Note these calculations have not used experimental conductivity data as input. The lower panel depicts the σ^{-1} dependence of predicted average solvation times for neat ILs and compares them with the correlation found from measurements with neat ILs. The comparison between theory²² and experiments²⁸ for neat ILs is performed to highlight that our calculations for neat ILs do predict the experimentally observed linear dependence on σ^{-1} and thus any deviation from this linearity for calculated average solvation times is specific for these binary mixtures and is not inherited from the calculations from neat ILs. It is clear from the upper panel that our calculated $\langle\tau_{\text{ss}}\rangle$ for ([Bmim][BF₄] + H₂O) mixtures deviate from the linear correlation (dashed lines) exhibited by those for neat ILs, although the extent of deviation does not appear to be as pronounced as observed in measurements.²³ Interestingly, our calculations indicate that at large x_{IL} ($x_{\text{IL}} > 0.5$) the contribution from ion structural relaxation ($\langle\tau_{\text{si}}\rangle$) dominates the average solvation times while the same is done by the dipolar relaxation part ($\langle\tau_{\text{sd}}\rangle$) at $x_{\text{IL}} \leq 0.5$. This is because in the present theory the contribution from ion structural relaxation has been fixed to 10% for neat IL which is then further proportionated to x_{IL} for these (IL + polar solvent) binary mixtures. The close agreement between theory and experiments seems to suggest that the ion structural relaxation component becomes nearly irrelevant at very low IL mole fractions because of low ion density but regains its importance with IL concentration through the increase of solution viscosity.

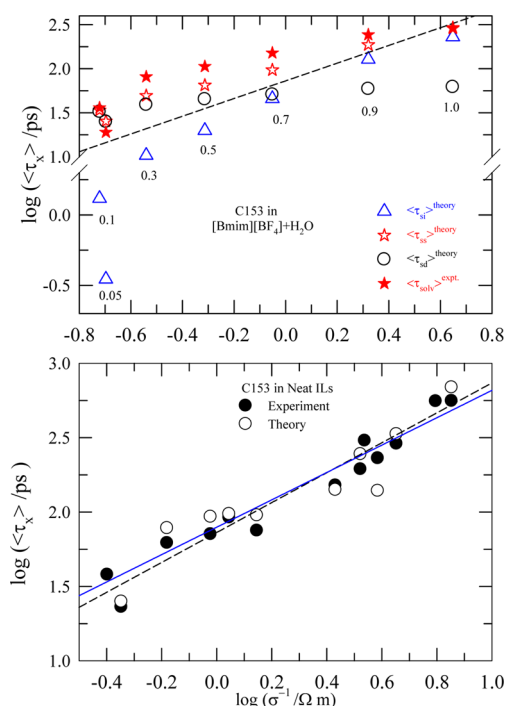


Figure 9. Dependence of average solvation times on inverse conductivity for C153 in ([Bmim][BF₄] + H₂O) mixtures (upper panel) and in neat ILs (lower panel). Open symbols in the upper panel denote EM predictions (without HF contribution in experimental $\epsilon(\omega)$), and the filled ones are from (FLUPS + TCSPC) measurements. Average times from other interaction contributions (mole fraction weighted) and IL mole fractions are also shown for facilitating analyses. The dashed line denotes the correlation curve drawn after considering both predicted and measured $\langle\tau_{\text{solv}}\rangle$. Open and filled circles in the lower panel represent, respectively, the predicted and measured $\langle\tau_{\text{solv}}\rangle$ for neat ILs with C153. While experimental data shown here are for 13 ILs (from ref 28), the predicted times are for 11 ILs (from ref 22). The solid line in the lower panel represents the correlation obtained in ref 30 after considering experimental data for 34 neat ILs. The dashed line is constructed after considering $\langle\tau_{\text{solv}}\rangle$ predicted for 11 neat ILs and measured for 13 neat ILs (see ref 28 for the identity of these ILs). Note $\langle\tau_{\text{sd}}\rangle^{\text{theory}} = (1 - 0.1x_{\text{IL}}) \int_0^\infty [x_{\text{IL}} S_{\text{sd}}(t) + (1 - x_{\text{IL}}) S_{\text{sp}}(t)] dt$ and $\langle\tau_{\text{si}}\rangle^{\text{theory}} = (0.1x_{\text{IL}}) \int_0^\infty S_{\text{si}} dt$.

IV. CONCLUSION

To summarize, the present work shows that the semimolecular theory developed earlier^{14–22} can be applied to successfully predict the composition dependent dynamic Stokes shift and average rate of solvation energy relaxation of a dissolved dipolar solute in (IL + polar solvent) binary mixtures. The mole fraction insensitivity of experimental shifts for both ([Bmim][BF₄] + H₂O) and ([Bmim][BF₄] + CH₃CN) binary mixtures has been reproduced by the present semimolecular theory after incorporating the volume disparity between the IL and the polar solvent molecules constituting the mixture. Two separate models—one that recognizes the separate identity of the added dipolar solvent molecules and the other that combines the separate dipolar species into one single effective dipolar entity—have been employed and the available experimental $\epsilon(\omega)$ ^{23,46} utilized for calculating both shifts and solvation response functions. Both model calculations provide a semi-quantitative description of the experimental viscosity dependence of the average slow times ($\langle\tau_s\rangle$) and mole fraction dependence of the average solvation rates ($\langle\tau_{\text{solv}}\rangle^{-1}$) for those mixtures reported by Liang et al. and Zhang et al. In addition,

these calculations have also highlighted the importance of the missing high frequency part of the dielectric relaxation for generating the ultrafast solvation time scales reported for these mixtures. In fact, when this missing component is included through some modeling, the present calculations are able to predict the experimentally observed sub-picosecond response in these mixtures at various compositions. The present calculations can also reproduce the experimentally observed nonlinearity in average solvation times when plotted as a function of the inverse of measured conductivity for these mixtures. This is a significant improvement over the dielectric continuum description which predicts a linear dependence. Several predictions have been made for these mixtures particularly at extremely dilute IL solutions which may be tested against experiments. The work described here also provides motivation for dielectric relaxation measurements with broader frequency coverage for these mixtures.

Even though the present work can successfully reproduce a number of experimental observations for these (IL + polar solvent) binary mixtures, there exists several demerits. For example, the spatial heterogeneity of these mixtures has not been included at all while performing the calculations. Spatial heterogeneity is an important issue for these mixtures, and systematic incorporation of this aspect should be done at the level of static solvent–solvent and solute–solvent correlations. The use of Gaussian decoupling approximation and the subsequent neglect of cross-terms while deriving the expression for the time dependent fluctuating solvation energy of dipolar solute in such binary mixtures is another aspect that requires improvement. Systematic incorporation of these aspects may be carried out by suitably expanding the present framework, but that would severely compromise the analytical simplicity and tractability of the current approach. In addition, the emergence of a nanosecond solvation component in measurements with neat IL and (IL + acetonitrile) mixtures needs to be understood in microscopic terms. Computer simulations⁷⁴ using realistic potentials may assist in understanding some of these aspects. A comparative understanding between the viscosity coupling of average solvation and rotation rates of a dipolar probe observed in (amide + electrolyte) deep eutectics^{75–78} and that in these binary mixtures, particularly at low IL mole fraction, would be highly stimulating, as both these systems possess spatial heterogeneity and similar longer-ranged interactions. A molecular level understanding of the interaction of water with imidazolium cation in (IL + water) mixtures as envisaged in Kerr spectroscopic studies^{79,80} constitutes an interesting problem which requires symbiosis between experiments and all-atom simulations. The study of dielectric relaxation of these mixtures using molecular theory⁸¹ is another challenging problem.

■ ASSOCIATED CONTENT

Supporting Information

Mixture composition dependent experimental densities, viscosity coefficients, and static dielectric constants for ([Bmim][BF₄] + CH₃CN) and ([Bmim][BF₄] + H₂O) binary mixtures, various interaction contributions calculated via EM and SM approaches for C153 in ([Bmim][BF₄] + H₂O) binary mixtures, wavenumber dependence of the effective static solute–solvent orientational correlation function at various IL mole fractions for the aqueous IL mixture, IL mole fraction dependent ion and dipole number densities used in our calculations, composition dependence of dipolar interaction

contribution to dynamic Stokes shift magnitudes predicted by SM and EM approaches, multiexponential fit parameters for the SM-predicted solvation response functions for C153 in ([Bmim][BF₄] + CH₃CN) and ([Bmim][BF₄] + H₂O) mixtures under various conditions, comparison of fit-functions used for fitting of calculated solvation response functions, sensitivity of calculated response functions toward different experimental dielectric relaxation data and water dipole moment dependence of it, viscosity dependence of average solvation times predicted at various IL mole fractions in these mixtures, and a scheme (Appendix 1) for the calculations of ion and dipole number densities required in EM calculations. This material is available free of charge via the Internet at <http://pubs.acs.org>.

AUTHOR INFORMATION

Corresponding Author

*E-mail: ranjit@bose.res.in. Phone: +91 33 2335 5706. Fax: +91 33 2335 3477.

Notes

The authors declare no competing financial interest.

ACKNOWLEDGMENTS

We thank Professor M. Maroncelli for prior sharing of experimental dynamic Stokes shift data for C153 in ([Bmim][BF₄] + CH₃CN) mixtures reported in ref 45. We thank anonymous reviewers for constructive suggestions that helped improve the quality of the manuscript. One of us (S.D.) thanks the Council of Scientific and Industrial Research (CSIR), India, for a research fellowship. The work reported here is supported partially by the TUE-CMS (SR/NM/NS-29/2011(G)) and UNANST projects at the Centre and a joint CSIR Project (01/(2558)12/EMR-II). We dedicate this work to Professor B. Bagchi for his continuous support and encouragement.

REFERENCES

- (1) Hynes, J. T. Chemical Reaction Dynamics in Solution. *Annu. Rev. Phys. Chem.* **1985**, *36*, 573–597.
- (2) Truhlar, D. G.; Hase, W. L.; Hynes, J. T. Current Status of Transition-State Theory. *J. Phys. Chem.* **1983**, *87*, 2664–2682.
- (3) Grote, R. F.; Hynes, J. T. The Stable States Picture of Chemical Reactions. II. Rate Constants for Condensed and Gas Phase Reaction Models. *J. Chem. Phys.* **1980**, *73*, 2715.
- (4) Bagchi, B.; Biswas, R. Polar and Nonpolar Solvation Dynamics, Ion Diffusion, and Vibrational Relaxation: Role of Biphasic Solvent Response in Chemical Dynamics. *Adv. Chem. Phys.* **1999**, *109*, 207–433.
- (5) Bagchi, B. Dynamics of Solvation and Charge Transfer Reactions in Dipolar Liquids. *Annu. Rev. Phys. Chem.* **1989**, *40*, 115–141.
- (6) Biswas, R.; Bagchi, B. Solvation Dynamics in Nonassociated Polar Solvents. *J. Phys. Chem. A* **1999**, *103*, 2495–2500.
- (7) Bagchi, B.; Chandra, A. Polarization Relaxation, Dielectric Dispersion, and Solvation Dynamics in Dense Dipolar Liquid. *J. Chem. Phys.* **1989**, *90*, 7338–7345.
- (8) Bagchi, B.; Jana, B. Solvation Dynamics in Dipolar Liquids. *Chem. Soc. Rev.* **2010**, *39*, 1936–1954.
- (9) Horng, M. L.; Gardecki, J. A.; Papazyan, A.; Maroncelli, M. Subpicosecond Measurements of Polar Solvation Dynamics: Coumarin 153 Revisited. *J. Phys. Chem.* **1995**, *99*, 17311–17337.
- (10) Richert, R.; Stickel, F.; Fee, R. S.; Maroncelli, M. Solvation Dynamics and the Dielectric Response in a Glass-Forming Solvent: From Picoseconds to Seconds. *Chem. Phys. Lett.* **1994**, *229*, 302–308.
- (11) Maroncelli, M.; Fleming, G. R. Picosecond Solvation Dynamics of Coumarin 153: The Importance of Molecular Aspects of Solvation. *J. Chem. Phys.* **1987**, *86*, 6221–6239.
- (12) Ito, N.; Duvvuri, K.; Matyushov, D. V.; Richert, R. Solvent Response and Dielectric Relaxation in Supercooled Butyronitrile. *J. Chem. Phys.* **2006**, *125*, 024504-1–024504-8.
- (13) Chandra, A.; Wei, D.; Patey, G. N. Dielectric Relaxation of Dipolar Liquids. *J. Chem. Phys.* **1993**, *99*, 2068–2073.
- (14) Kashyap, H. K.; Biswas, R. Dipolar Solvation Dynamics in Room Temperature Ionic Liquids: An Effective Medium Calculation Using Dielectric Relaxation Data. *J. Phys. Chem. B* **2008**, *112*, 12431–12438.
- (15) Kashyap, H. K.; Biswas, R. Solvation Dynamics of Dipolar Probes in Dipolar Room Temperature Ionic Liquids: Separation of Ion-Dipole and Dipole-Dipole Interaction Contributions. *J. Phys. Chem. B* **2010**, *114*, 254–268.
- (16) Kashyap, H. K.; Biswas, R. Solvation Dynamics in Imidazolium and Phosphonium Ionic Liquids: Effects of Solute Motion. *Indian J. Chem.* **2010**, *49A*, 685–694.
- (17) Kashyap, H. K.; Biswas, R. Stokes' Shift Dynamics in Imidazolium Ionic Liquids: Temperature Dependence. *J. Phys. Chem. B* **2010**, *114*, 16811–16823.
- (18) Daschakraborty, S.; Biswas, R. Stokes' Shift Dynamics in (Ionic Liquid + Polar Solvent) Binary Mixtures: Composition Dependence. *J. Phys. Chem. B* **2011**, *115*, 4011–4024.
- (19) Daschakraborty, S.; Biswas, R. Stokes' Shift Dynamics in Alkylimidazolium Aluminate Ionic Liquids: Domination of Solute-IL Dipole-Dipole Interaction. *Chem. Phys. Lett.* **2011**, *510*, 202–207.
- (20) Daschakraborty, S.; Biswas, R. Stokes Shift Dynamics of [Na][TOTO] - A New Class of Ionic Liquids: A Comparative Study with More Common Imidazolium Analogs. *Chem. Phys. Lett.* **2012**, *545*, 54–59.
- (21) Daschakraborty, S.; Biswas, R. Ultrafast Solvation Response in Room Temperature Ionic Liquids: Possible Origin, and Importance of the Collective and the Nearest Neighbour Solvent Modes. *J. Chem. Phys.* **2012**, *137*, 114501-1–114501-11.
- (22) Daschakraborty, S.; Pal, T.; Biswas, R. Stokes shift Dynamics of Ionic Liquids: Solute Probe Dependence, and Effects of Self-Motion, Dielectric Relaxation Frequency Window and Collective Intermolecular Solvent Modes. *J. Chem. Phys.* **2013**, *139*, 164503-1–164503-12.
- (23) Zhang, X.-X.; Liang, M.; Hunger, J.; Buchner, R.; Maroncelli, M. Dielectric Relaxation and Solvation Dynamics in a Prototypical Ionic Liquid + Dipolar Protic Liquid Mixture: 1-Butyl-3-Methylimidazolium Tetrafluoroborate + Water. *J. Phys. Chem. B* **2013**, *117*, 15356–15368.
- (24) Halder, M.; Headley, L. S.; Mukherjee, P.; Song, X.; Petrich, J. W. Experimental and Theoretical Investigations of Solvation Dynamics of Ionic Fluids: Appropriateness of Dielectric Theory and the Role of DC Conductivity. *J. Phys. Chem. A* **2006**, *110*, 8623–8626.
- (25) Arzhantsev, S.; Jin, H.; Baker, G. A.; Maroncelli, M. Measurements of the Complete Solvation Response in Ionic Liquids. *J. Phys. Chem. B* **2007**, *111*, 4978–4989.
- (26) Song, X. Solvation Dynamics in Ionic Fluids: An Extended Debye–Hückel Dielectric Continuum Model. *J. Chem. Phys.* **2009**, *131*, 044503-1–044503-8.
- (27) Maroncelli, M.; Zhang, X.-X.; Liang, M.; Roy, D.; Ernstring, N. P. Measurements of the Complete Solvation Response of Coumarin 153 in Ionic Liquids and the Accuracy of Simple Dielectric Continuum Predictions. *Faraday Discuss.* **2012**, *154*, 409–424.
- (28) Zhang, X.-X.; Liang, M.; Ernstring, N. P.; Maroncelli, M. Complete Solvation Response of Coumarin 153 in Ionic Liquids. *J. Phys. Chem. B* **2013**, *117*, 4291–4304.
- (29) Zhang, X.-X.; Schroder, C.; Ernstring, N. P. Solvation and Dielectric Response in Ionic Liquids—Conductivity Extension of the Continuum Model. *J. Chem. Phys.* **2013**, *138*, 111102-1–111102-3.
- (30) Zhang, X.-X.; Liang, M.; Ernstring, N. P.; Maroncelli, M. Conductivity and Solvation Dynamics in Ionic Liquids. *J. Phys. Chem. Lett.* **2013**, *4*, 1205–1210.
- (31) Shim, Y.; Kim, H. J. Dielectric Relaxation, Ion Conductivity, Solvent Rotation, and Solvation Dynamics in a Room-Temperature Ionic Liquid. *J. Phys. Chem. B* **2008**, *112*, 11028–11038.

- (32) Shim, Y.; Kim, H. J. Dielectric Relaxation and Solvation Dynamics in a Room-Temperature Ionic Liquid: Temperature Dependence. *J. Phys. Chem. B* **2013**, *117*, 11743–11752.
- (33) Samanta, A. Solvation dynamics in ionic liquids: What We Have Learned From the Dynamic Fluorescence Stokes Shift Studies. *J. Phys. Chem. Lett.* **2010**, *1*, 1557–1562.
- (34) Samanta, A. Dynamic Stokes Shift and Excitation Wavelength Dependent Fluorescence of Dipolar Molecules in Room Temperature Ionic Liquids. *J. Phys. Chem. B* **2006**, *110*, 13704–13716.
- (35) Das, S. K.; Sahu, P. K.; Sarkar, M. Diffusion–Viscosity Decoupling in Solute Rotation and Solvent Relaxation of Coumarin-153 in Ionic Liquids Containing Fluoroalkylphosphate (FAP) Anion: A Thermophysical and Photophysical Study. *J. Phys. Chem. B* **2013**, *117*, 636–647.
- (36) Das, S. K.; Sarkar, M. Studies on the Solvation Dynamics of Coumarin 153 in 1-Ethyl-3-Methylimidazolium Alkylsulfate Ionic Liquids: Dependence on Alkyl Chain Length. *ChemPhysChem* **2012**, *13*, 2761–2768.
- (37) Das, S. K.; Sahu, P. K.; Sarkar, M. Probing the Microscopic Aspects of 1-Butyl-3-Methylimidazolium Trifluoroacetate Ionic Liquid and Its Mixture with Water and Methanol: A Photophysical and Theoretical (DFT) Study. *J. Fluoresc.* **2013**, *23*, 1217–1227.
- (38) Terranova, Z. L.; Corcelli, S. A. On the Mechanism of Solvation Dynamics in Imidazolium-Based Ionic Liquids. *J. Phys. Chem. B* **2013**, *117*, 15659–15666.
- (39) Chakrabarty, D.; Chakraborty, A.; Seth, D.; Hazra, P.; Sarkar, N. Dynamics of Solvation and Rotational Relaxation of Coumarin 153 in 1-Butyl-3-Methylimidazolium Hexafluorophosphate [Bmim][PF₆]-Water Mixtures. *Chem. Phys. Lett.* **2004**, *397*, 469–474.
- (40) Chakrabarty, D.; Chakraborty, A.; Seth, D.; Sarkar, N. Effect of Water, Methanol, and Acetonitrile on Solvent Relaxation and Rotational Relaxation of Coumarin 153 in Neat 1-Hexyl-3-methylimidazolium Hexafluorophosphate. *J. Phys. Chem. A* **2005**, *109*, 1764–1769.
- (41) Sarkar, S.; Pramanik, R.; Ghatak, C.; Setua, P.; Sarkar, N. Probing the Interaction of 1-Ethyl-3-methylimidazolium Ethyl Sulfate ([Emim][EtSO₄]) with Alcohols and Water by Solvent and Rotational Relaxation. *J. Phys. Chem. B* **2010**, *114*, 2779–2789.
- (42) Baker, S. N.; Baker, G. A.; Munson, C. A.; Chen, F.; Bukwoski, E. J.; Cartwright, A. N.; Bright, F. V. Effects of Solubilized Water on the Relaxation Dynamics Surrounding 6-Propionyl-2-(*N,N*-dimethylamino)naphthalene Dissolved in 1-Butyl-3-methylimidazolium Hexafluorophosphate at 298 K. *Ind. Eng. Chem. Res.* **2003**, *42*, 6457–6463.
- (43) Pramanik, R.; Rao, V. G.; Sarkar, S.; Ghatak, C.; Setua, P.; Sarkar, N. Effects of Solubilized Water on the Relaxation Dynamics Surrounding 6-Propionyl-2-(*N,N*-dimethylamino)naphthalene Dissolved in 1-Butyl-3-methylimidazolium Hexafluorophosphate at 298 K. *J. Phys. Chem. B* **2009**, *113*, 8626–8634.
- (44) Annappureddy, H. V. R.; Hu, Z.; Xia, J.; Margulis, C. J. How Does Water Affect the Dynamics of the Room-Temperature Ionic Liquid 1-Hexyl-3-methylimidazolium Hexafluorophosphate and the Fluorescence Spectroscopy of Coumarin-153 When Dissolved in It? *J. Phys. Chem. B* **2008**, *112*, 1770–1776.
- (45) Liang, M.; Zhang, X.-X.; Kaintz, A.; Ernsting, N. P.; Maroncelli, M. Solvation Dynamics in a Prototypical Ionic Liquid + Dipolar Aprotic Liquid Mixture: 1-Butyl-3-Methylimidazolium Tetrafluoroborate + Acetonitrile. *J. Phys. Chem. B* **2013**, DOI: 10.1021/jp412086t.
- (46) Stoppa, A.; Hunger, J.; Hefter, G.; Buchner, R. Structure and Dynamics of 1-*N*-Alkyl-3-*N*-Methylimidazolium Tetrafluoroborate + Acetonitrile Mixtures. *J. Phys. Chem. B* **2012**, *116*, 7509–7521.
- (47) Saha, S.; Mandal, P. K.; Samanta, A. Solvation Dynamics of Nile Red in a Room Temperature Ionic Liquid Using Streak Camera. *Phys. Chem. Chem. Phys.* **2004**, *6*, 3106–3110.
- (48) Wang, Y.; Voth, G. A. Unique Spatial Heterogeneity in Ionic Liquids. *J. Am. Chem. Soc.* **2005**, *127*, 12192–12193.
- (49) Triolo, A.; Russina, O.; Fazio, B.; Triolo, R.; Di Cola, E. Morphology of 1-Alkyl-3-Methylimidazolium Hexafluorophosphate Room Temperature Ionic Liquids. *Chem. Phys. Lett.* **2008**, *457*, 362–365.
- (50) Mandal, P. K.; Sarkar, M.; Samanta, A. Excitation-Wavelength-Dependent Fluorescence Behavior of Some Dipolar Molecules in Room-Temperature Ionic Liquids. *J. Phys. Chem. A* **2004**, *108*, 9048–9053.
- (51) Jin, H.; Li, X.; Maroncelli, M. Heterogeneous Solute Dynamics in Room Temperature Ionic Liquids. *J. Phys. Chem. B* **2007**, *111*, 13473–13478.
- (52) Adhikari, A.; Sahu, A. K.; Dey, S.; Ghose, S.; Mandal, U.; Bhattacharyya, K. Femtosecond Solvation Dynamics in a Neat Ionic Liquid and Ionic Liquid Microemulsion: Excitation Wavelength Dependence. *J. Phys. Chem. B* **2007**, *111*, 12809.
- (53) Hu, Z.; Margulis, C. J. Heterogeneity in a Room-Temperature Ionic Liquid: Persistent Local Environments and the Red-Edge Effect. *Proc. Natl. Acad. Sci. U.S.A.* **2006**, *103*, 831.
- (54) Castner, E. W., Jr.; Margulis, C. J.; Maroncelli, M.; Wishart, J. F. Ionic Liquids: Structure and Photochemical Reactions. *Annu. Rev. Phys. Chem.* **2011**, *62*, 85–105.
- (55) Roy, S.; Bagchi, B. Solvation Dynamics in Liquid Water. A Novel Interplay Between Librational and Diffusive modes. *J. Chem. Phys.* **1993**, *99*, 9938–9943.
- (56) Roy, S.; Bagchi, B. Ultrafast Underdamped Solvation: Agreement Between Computer Simulation and Various Theories of Solvation Dynamics. *J. Chem. Phys.* **1993**, *99*, 1310–1319.
- (57) Biswas, R.; Bagchi, B. Self-Consistent Microscopic Treatment of the Effects of Self-Motion of the Probe on Ionic and Dipolar Solvation Dynamics. *J. Phys. Chem.* **1996**, *100*, 4261–4268.
- (58) Biswas, R.; Bagchi, B. Solvation Dynamics in Slow, Viscous Liquids: Application to Amides. *J. Phys. Chem.* **1996**, *100*, 1238–1245.
- (59) Gray, C. G.; Gubbins, K. E. *Theory of Molecular Fluids*; Clarendon: Oxford, U.K., 1984; Vol. I.
- (60) Hansen, J. P.; McDonald, I. R. *Theory of Simple Liquids*; Academic Press: London, 1986.
- (61) Labowitz, J. L. Exact Solution of Generalized Percus-Yevick Equation for a Mixture of Hard Spheres. *Phys. Rev.* **1964**, *133*, A895–A899.
- (62) Attard, P. Asymptotic Analysis of Primitive Model Electrolytes and the Electrical Double Layer. *Phys. Rev. E* **1993**, *48*, 3604–3621.
- (63) Chandra, A.; Bagchi, B. Ion Conductance in Electrolyte Solutions. *J. Chem. Phys.* **1999**, *110*, 10024–10034.
- (64) Kindt, J. T.; Schmittenmaer, C. A. Far-Infrared Dielectric Properties of Polar Liquids Probed by Femtosecond Terahertz Pulse Spectroscopy. *J. Phys. Chem.* **1996**, *100*, 10373–10379.
- (65) Kemp, D. D.; Gordon, M. S. An Interpretation of the Enhancement of the Water Dipole Moment Due to the Presence of Other Water Molecules. *J. Phys. Chem. A* **2008**, *112*, 4885–4894.
- (66) Gubskaya, A. V.; Kushalik, P. J. The Total Molecular Dipole Moment for Liquid Water. *J. Chem. Phys.* **2002**, *117*, 5290–5302.
- (67) Jellema, R.; Bulthuis, J.; van der Zwan, G. Dielectric Relaxation of Acetonitrile-Water Mixtures. *J. Mol. Liq.* **1997**, *73–74*, 179–193.
- (68) Wang, J.; Tian, Y.; Zhao, Y.; Zhuo, K. A Volumetric and Viscosity Study for the Mixtures of 1-*n*-Butyl-3-methylimidazolium Tetrafluoroborate Ionic Liquid with Acetonitrile, Dichloromethane, 2-Butanone and *N,N*-Dimethylformamide. *Green Chem.* **2003**, *5*, 618–622.
- (69) Chapman, C. F.; Maroncelli, M. Fluorescence Studies of Solvation and Solvation Dynamics in Ionic Solutions. *J. Phys. Chem.* **1991**, *95*, 9095–9114.
- (70) Nakamura, K.; Shikata, T. Systematic Dielectric and NMR Study of the Ionic Liquid 1-Alkyl-3-Methyl Imidazolium. *ChemPhysChem* **2010**, *11*, 285–294.
- (71) Soriano, A. N.; Doma, B. T.; Li, M.-H. Measurements of the density and refractive index for 1-*n*-Butyl-3-Methylimidazolium-based Ionic Liquids. *J. Chem. Thermodyn.* **2009**, *41*, 301–307.
- (72) Ohba, T.; Ikawa, S. Far-infrared Optical Constants of Liquid Acetonitrile at 238 to 343 K as Measured with a Synchrotron Radiation Source. *Mol. Phys.* **1991**, *73*, 985–997.

- (73) Hunger, J.; Stoppa, A.; Schrodle, S.; Hefter, G.; Buchner, R. Temperature Dependence of the Dielectric Properties and Dynamics of Ionic Liquids. *ChemPhysChem* **2009**, *10*, 723–733.
- (74) Pal, T.; Biswas, R. Rank-dependent Orientational Relaxation in an Ionic Liquid: An All-Atom Simulation Study. *Theor. Chem. Acc.* **2013**, *132*, 1348-1–1348-12.
- (75) Guchhait, B.; Gazi, H. A. R.; Kashyap, H. K.; Biswas, R. Fluorescence Spectroscopic Studies of (Acetamide + Sodium/Potassium Thiocyanates) Molten Mixtures: Composition and Temperature Dependence. *J. Phys. Chem. B* **2010**, *114*, 5066–5081.
- (76) Guchhait, B.; Daschakraborty, S.; Biswas, R. Medium Decoupling of Dynamics at Temperatures ~ 100 K Above Glass Transition Temperature: A Case Study with (Acetamide + Lithium Bromide/Nitrate) Melts. *J. Chem. Phys.* **2012**, *136*, 174503-1–174503-16.
- (77) Pal, T.; Biswas, R. Heterogeneity and Viscosity Decoupling in (Acetamide + Electrolyte) Molten Mixtures: A Model Simulation Study. *Chem. Phys. Lett.* **2011**, *517*, 180–185.
- (78) Das, A.; Das, S.; Biswas, R. Fast Fluctuations in Deep Eutectic Melts: Multi-probe Fluorescence Measurements and All-Atom Molecular Dynamics Simulation Study. *Chem. Phys. Lett.* **2013**, *581*, 47–51.
- (79) Sturlaugson, A. L.; Fruchey, K. S.; Fayer, M. D. Orientational Dynamics of Room Temperature Ionic Liquid/ Water Mixtures: Water-induced Structure. *J. Phys. Chem. B* **2012**, *116*, 1777–1787.
- (80) Shirota, H.; Biswas, R. Intermolecular/Interionic Vibrations of 1-Methyl-3-n-Octylimidazolium Tetrafluoroborate Ionic Liquid and H₂O Mixtures. *J. Phys. Chem. B* **2012**, *116*, 13765–13773.
- (81) Daschakraborty, S.; Biswas, R. Dielectric Relaxation in Ionic Liquids: Role of Ion-Ion and Ion-Dipole Interactions, and Effects of Heterogeneity. *J. Chem. Phys.* **2014**, *140*, 014504-1–014504-12.